AIP | The Journal of Chemical Physics

Improved sliced velocity map imaging apparatus optimized for H photofragments

Mikhail Ryazanov and Hanna Reisler

Citation: J. Chem. Phys. **138**, 144201 (2013); doi: 10.1063/1.4798929
View online: http://dx.doi.org/10.1063/1.4798929
View Table of Contents: http://jcp.aip.org/resource/1/JCPSA6/v138/i14
Published by the American Institute of Physics.

Improved sliced velocity map imaging apparatus optimized for H photofragments

Mikhail Ryazanov[a] and Hanna Reisler[b]
Department of Chemistry, University of Southern California, Los Angeles, California 90089-0482, USA

(Received 24 November 2012; accepted 9 March 2013; published online 10 April 2013)

Time-sliced velocity map imaging (SVMI), a high-resolution method for measuring kinetic energy distributions of products in scattering and photodissociation reactions, is challenging to implement for atomic hydrogen products. We describe an ion optics design aimed at achieving SVMI of H fragments in a broad range of kinetic energies (KE), from a fraction of an electronvolt to a few electronvolts. In order to enable consistently thin slicing for any imaged KE range, an additional electrostatic lens is introduced in the drift region for radial magnification control without affecting temporal stretching of the ion cloud. Time slices of ~5 ns out of a cloud stretched to ≥50 ns are used. An accelerator region with variable dimensions (using multiple electrodes) is employed for better optimization of radial and temporal space focusing characteristics at each magnification level. The implemented system was successfully tested by recording images of H fragments from the photodissociation of HBr, H_2S, and the CH_2OH radical, with kinetic energies ranging from <0.4 eV to >3 eV. It demonstrated KE resolution ≲1%–2%, similar to that obtained in traditional velocity map imaging followed by reconstruction, and to KE resolution achieved previously in SVMI of heavier products. We expect it to perform just as well up to at least 6 eV of kinetic energy. The tests showed that numerical simulations of the electric fields and ion trajectories in the system, used for optimization of the design and operating parameters, provide an accurate and reliable description of all aspects of system performance. This offers the advantage of selecting the best operating conditions in each measurement without the need for additional calibration experiments. © *2013 American Institute of Physics*. [http://dx.doi.org/10.1063/1.4798929]

I. INTRODUCTION

Velocity map imaging (VMI) is a widely used technique for determining velocity distributions in photoinitiated fragmentation, ionization, electron detachment, and reactive scattering processes.[1,2] In the years since 1997, when Eppink and Parker[3] had introduced the ion optics arrangement that significantly reduced spatial blurring in velocity imaging,[4] additional improvements further increased resolution and sensitivity, as summarized in several monographs and reviews.[1,2,5,6] In the Eppink–Parker VMI implementation, the three-dimensional (3D) velocity distribution is projected onto a position-sensitive detector, producing a two-dimensional (2D) image. To retrieve the original 3D velocity distribution, image reconstruction (inverse Abel transform) is required. While fast and efficient reconstruction implementations do exist, they require cylindrical symmetry of the original 3D distribution and lead to unfavorable redistribution of the experimental noise, which may limit resolution in specific regions of the image.[6]

For situations where a cylindrical symmetry is absent, or "zooming" on low-velocity regions of the distribution is needed, avoiding image reconstruction is advantageous. Ideally, recording of all three velocity vector components in coincidence for each fragment would give the complete 3D velocity distribution directly. This can be achieved straightforwardly under single-particle detection conditions, but in that case signal levels are low, and hence acquisition times to obtain the complete distribution might be exceedingly long. As another approach, sliced velocity map imaging (SVMI) methods that select thin 2D slices out of the 3D velocity distribution for direct analysis have been developed.[7–9] In photodissociation experiments with cylindrical symmetry the slice parallel to the symmetry axis (laser polarization direction) and passing through the center of the velocity distribution provides complete information about the original 3D distribution with no need for reconstruction. Of the variants of this method,[1] the time-slicing technique based on electrostatic ion optics[8,9] is easiest to implement and features excellent signal-to-noise ratios as well as high sensitivity and resolution. It is now used routinely in monitoring atomic and molecular dissociation fragments that can be detected by state-specific ionization, and is our chosen method.

SVMI systems map two initial velocity components of the ion to arrival position at the detector, whereas the third (axial, perpendicular to the detector) component is mapped to the arrival time. Slicing is achieved by fast gating of the detector. This requires time-stretching of the fragment ion cloud to an extent that the gating pulse can select about a tenth of the cloud. For the 20–30 ns gating pulses available from commercial pulse generators such stretching is fairly easy to achieve for all ionic fragments except atomic hydrogen. The mass-dependence of the stretching (see below) makes SVMI of H

[a]Present address: Lawrence Berkeley National Laboratory, Berkeley, California 94720, USA. Electronic mail: mikhail.ryazanov@gmail.com
[b]Electronic mail: reisler@usc.edu

photofragments more difficult, requiring even faster gating, and almost impossible for photoelectrons.

H atoms are important fragments in many dissociation processes, such as those encountered in combustion and atmospheric reactions. They are also generated in photoinitiated decomposition of many hydrocarbon radicals. However, determining their kinetic energy distributions poses some complications. In free radicals, because of the existence of numerous low-lying excited electronic states, spurious multiphoton processes can give rise to energetic H fragments in addition to the signal from the studied one-photon process. When using full-projection VMI, it is mandatory to record an image of the entire distribution because high-velocity signals have projections into the low-velocity region and must be separated from the low-velocity signals by reconstruction. The experimental noise from such projections, however, cannot be separated and leads to masking of weak one-photon signals. At the same time, SVMI separates contributions from different velocities experimentally. This allows "zooming" solely on low-velocity regions, thereby efficiently eliminating contributions from high-energy processes.

However, as mentioned before, practical implementation of SVMI for hydrogen fragments is complicated by high temporal requirements, and most SVMI setups currently in use are not able to perform adequate slicing for these light ions or can do it only for a very limited kinetic energy range (see Refs. 10–12 for a few examples and Sec. IV for more details). The present work demonstrates that significant improvements can be made in this respect. The purely electrostatic ion optics design described here is optimized for SVMI of H photofragments under a broad range of conditions. Incorporation of an additional lens in the drift region greatly enhances the control of image magnification[13] without introducing significant deterioration of resolution and thus permits to use lower electric fields in the ionization region in order to achieve larger time stretchings.[14] The design allows to obtain high-resolution sliced images for H photofragments ranging in kinetic energy (KE) from ∼0.1 to ∼6 eV. Like other VMI and SVMI systems, the present setup can be used for detection of ions of different masses as well. Its mass resolution is sufficient for all experiments with small organic molecules.

Optimal parameters of the ion optics were determined by numerical simulations aiming at maximum quality of radial and time-of-flight (TOF) focusing with respect to initial ion positions for an ion source region with real-world parameters. Experimental tests demonstrated that these simulations predict the behavior of the actual system so reliably that the simulated parameters can be used in SVMI measurements without additional experimental adjustments and calibrations. The criteria developed in this work are general and can be incorporated into different instrument designs. Due to the limited size of this article, only the most important aspects will be discussed below, but more details can be found in Ref. 15 or on our website.[16]

II. ION OPTICS DESIGN

As described above, the primary design goal for the new system was the ability to perform SVMI of atomic hydrogen products from photodissociation of small organic radicals. Kinetic energy release in such processes ranges from a fraction of an electronvolt to a few electronvolts, and due to the large mass difference between the H fragment and the molecular cofragment, almost all the kinetic energy is carried by the H atom.

The designed SVMI system had to fit into an existing molecular beam apparatus,[17] which imposed several geometric constraints on the ion optics. In particular, the ∼15 cm inner diameter of the vacuum chamber limited the radial size of the ion optics elements. Another important geometrical parameter was the detector diameter. Since the multichannel plate (MCP) detector assembly is the most expensive part of the SVMI system and the only part that has a finite lifetime and thus has to be replaced periodically, it was decided to employ the same ø40 mm double-stack MCP detector type as in the other VMI setup[18] in our laboratory.

A. Choice of SVMI approach

Before considering the details of the ion-optical arrangement, the choice between the two major SVMI approaches—with the so-called "delayed extraction"[7] and with purely electrostatic lenses[8,9]—needs to be explained. While the former in principle allows arbitrarily large TOF stretching by using very long delays, the fast nature of the light H^+ ions demands finely controlled (with nanosecond precision) switching of the kilovolt-range voltages applied to the ion optics. Since electromagnetic waves propagate through the system (the ion optics and the vacuum chamber) at speed no faster than 30 cm/ns, the transient processes in a system of a usual size would take no less than a few nanoseconds.[19] That is, rational design of such a system for reliable operation might require solution of the time-dependent Maxwell equations in nontrivial geometry and with real nonperfect conductors and dielectrics, which is an intricate task.

Moreover, the delayed extraction approach is based on mapping the ion *positions* in the expanded cloud to the arrival times. It means that the setup must not satisfy Wiley–McLaren conditions[20] for TOF spatial focusing, and thus the initial positions of ions within the ionization volume will contribute to their arrival times, deteriorating the time resolution of the system and hence its SVMI performance. Although the "time-lag energy focusing" mentioned in Ref. 20 indicates that delayed extraction allows separate control of arrival time dependences on initial positions and velocities, we were not aware of studies regarding the possibility of retaining space focusing while maximizing TOF dispersion with respect to the initial velocity.

In addition, we had no prior experience in our laboratory with the delayed extraction method. Therefore, for us the simplest and most robust method of achieving velocity mapping with both radial and TOF spatial focusing was the approach based on electrostatic ion optics (with time-independent electric potential). The overall arrangement of the system was determined based on general properties of electrostatic lenses, and the specific parameters

were then optimized using the ion optics simulation software package SIMION 8[21,22] complemented with customized user-programming scripts for analysis of the ion trajectories and (semi)automatic optimization of the electric field parameters.[16]

B. TOF stretching

The temporal requirements for SVMI are dictated by the time resolution of the experiment. The experiments in our laboratory are carried out with ionizing laser pulses of several-nanosecond duration, which limits the overall time resolution of the experiment. Effective relative slice thickness ~1/10, which is required for good resolution, therefore demands TOF stretching for the imaged velocity range of the order of a few tens of nanoseconds. Satisfying this criterion for light H ions constitutes the main difficulty in implementing SVMI in our case.

Although thin slicing requires fast gating of the detector, using detector-gating pulses shorter than the laser pulse duration will not lead to an improvement in resolution but only to a decrease in signal intensity. Therefore, a suitable high-voltage pulser for gating the MCP detector was developed. It constitutes a downscaled version of a fast megavolt-range pulser based on magnetic pulse compression and diode recovery switching[23] (see also Ref. 24) and delivers electrical pulses with amplitudes up to ~2 kV and halfwidth of ~5 ns to the MCP stack.

The effective slicing pulse, determined by the convolution of the ionization intensity time profile, the detector gain time profile, and the relative timing jitter distribution, is somewhat narrowed compared to the laser and electric pulses due to nonlinearities in the ionization process, as well as in the voltage–gain dependence of the detector. The actual time-slicing profile, experimentally measured by observing the detected intensity of photoelectrons as a function of the delay between the laser and the slicing pulser triggers, has a nearly Gaussian shape with a halfwidth of 4–5 ns. This is somewhat narrower than the results obtained by using MOSFET[25] and avalanche-transistor[26] pulsers.

The ~1/10 relative slicing thickness thus requires TOF stretching of ~50 ns for the studied ions. It can be shown that in electrostatic ion-optical systems suitable for SVMI applications the TOF stretching for a cloud of ions of mass m with initial kinetic energy K_0 is

$$\Delta\tau = \frac{2\sqrt{2mK_0}}{qE_0}, \tag{1}$$

where q is the ion charge, and E_0 is the electric field strength in the ionization region. Note that this *local* field is *the only* ion optics parameter that controls the TOF dispersion of the SVMI system. For example, 50 ns stretching for 1 eV H^+ ions requires $E_0 \approx 58$ V/cm. The objective of the SVMI ion optics design is therefore to fulfill the spatial focusing conditions while producing an image of the desired size on the detector at a given E_0 value.

C. Radial magnification

The image size also depends on the initial kinetic energies of the ions, having the same $\sqrt{K_0}$ proportionality as in (1), but in fixed electric field configuration it is inversely proportional to the square root of the ion optics voltages. That is, the radial magnification has $1/\sqrt{E_0}$ dependence, which is different from that of the TOF dispersion ($1/E_0$). This fact has important implications for SVMI systems: adjustments of voltages in order to fit an image of ions with a given KE range into the detector strongly affect the TOF stretching, so that if the system produces 50 ns stretching for 1 eV ions, the stretching for 2 eV ions will be only 25 ns, which is not sufficient for slicing. On the other hand, stretching for ions with lower KEs will be proportionally larger, leading to excessively thin slices[27] and hence decreased collection efficiency. Therefore, some means for radial magnification control independent of the electric field in the ionization region are desired, and their implementation requires variable field geometry.

The minimal ion-optical system that can achieve spatial focusing for both radial (Eppink–Parker[3]) and temporal (Wiley–McLaren[20]) parts of velocity mapping can be based on 2-aperture Eppink–Parker arrangement[3] consisting of 3 electrodes (see Fig. 1(a)). Besides the electric field E_0 in the ionization region (between the first two electrodes), which is dictated by the desired TOF dispersion, such a system has 3 parameters: the second electric field E_1 (between the last two electrodes), and the two distances L_0 and L_1 between the electrodes. The radial and temporal focusing conditions form two independent equations that must be solved with respect to these three variables. This leaves one degree of freedom, which can be used for magnification control. However, as the examples of numerical simulations presented in Fig. 1 show, the available magnification range is rather limited, such that only ~20% variation can be achieved at the price of about 3-fold deterioration of focusing quality.

D. Compound electrostatic lens

A natural way to improve the performance is by adding more electrodes to the ion-optical system. This should extend the flexibility of the electric field configurations and increase the number of free parameters subject to optimization. Some SVMI systems[9,28] indeed use more than two apertures; however no detailed discussion regarding the selection criteria of the employed arrangements and their parameters has been given. Therefore, below we analyze the general properties of a simple ion-optical system consisting of the Eppink–Parker arrangement (referred to as "accelerator" henceforth) and one more unipotential electrostatic lens (referred to simply as the "lens").

As already mentioned, the TOF dispersion of the system is not affected by the electrostatic field configuration outside the ionization region, and thus only the effect of the lens on the radial magnification has to be studied. Under the assumption that both the accelerator and the lens are much thinner than the total TOF length, and that small deviations from focusing conditions of the accelerator have little effect on its

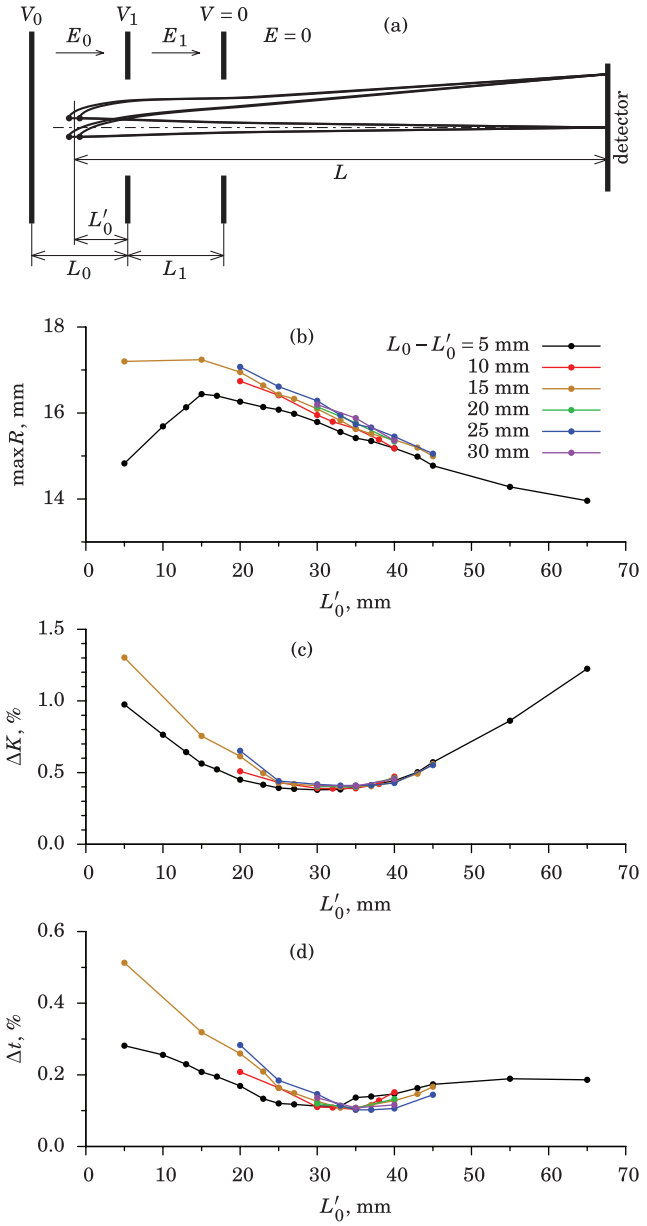

FIG. 1. Minimal SVMI system with 3-electrode ion optics and its performance characteristics under simultaneous TOF and radial focusing conditions: (a) cross-section diagram, (b) image radius for 1 eV ions, (c) relative radial blurring in the KE scale, (d) relative TOF blurring. (The distance L'_0 between the ionization region and the second electrode was chosen as the independent parameter for plotting. E_0 was fixed at 58 V/cm for 50 ns TOF stretching. Total TOF length $L = 60$ cm.)

radial magnification, simple ray optics considerations (see also an illustrative drawing in supplementary material[29]) yield the following expressions for the lens focal length required to satisfy the net focusing:

$$f_l = l\left(1 - \frac{l}{L - F_R}\right) \tag{2}$$

and for the resulting magnification change:

$$M_{\text{rel}} \equiv \frac{R'}{R} = -\frac{F_R l}{L(L - l - F_R)}, \tag{3}$$

where R and R' are image radii with and without the lens, respectively, L is the field-free TOF length, l is the distance from the detector plane to the lens, and F_R is the focal length of the accelerator. Since addition of the lens changes the overall beam focusing, F_R (which is equal to L in operation without the lens) must be matched to the lens parameters when using the lens. The properties of the Eppink–Parker arrangement do not allow the accelerator to be strongly diverging (small negative F_R), and operation with strong convergence (small positive F_R) generally leads to large aberrations and hence poor resolution. Therefore, the challenge is to find the best position of the lens[30] that will allow the broadest M_{rel} range corresponding to a limited variation of the accelerator optical power.

For example, limiting

$$-\frac{1}{L} \le \frac{1}{F_R} \le \frac{1}{L} \tag{4}$$

leads, by (2) and (3), to

$$\frac{l}{2L - l} \le M_{\text{rel}} \le 1, \tag{5}$$

$$l\left(1 - \frac{l}{2L}\right) \le f_l \le +\infty. \tag{6}$$

These results clearly indicate that the maximum reduction of radial magnification can be achieved if the lens is placed *closer to the detector* ($l \ll L$ in (5)) and has short focus ($f_l \approx l$, from (6)). The smallness of l is, however, limited by the fact that the ion beam diameter at the lens will be approximately $\frac{1}{M_{\text{rel}}}\frac{L-l}{L}$ times larger than the image diameter at the detector, and thus in case of small $f_l \approx l$ the lens must work at very high relative apertures, significantly increasing the aberrations. The conclusion is therefore that the additional lens for magnification control should be located somewhere in the TOF tube, far from the accelerator but not too close to the detector. Filling factor considerations suggest that a cylindrical lens is preferred over an aperture lens as it would have much smaller overall radial size for the same aperture diameter.

In our implementation the total TOF length of the experimental setup was set at $L \approx 63$ cm,[31] which gave suitable radial magnification for low-KE ions and sufficient mass resolution in TOF mass-spectrometer mode of operation. The additional unipotential lens of the "standard" cylindrical type (with lengths of all 3 electrodes equal to the aperture diameter) was placed at a distance $l \approx L/3$ from the detector, as shown in Fig. 2. Given the vacuum chamber dimensions, a maximum feasible aperture diameter of 120 mm was used in order to keep the lens filling factor as low as possible.

As seen on the left in Fig. 2, an accelerator consisting of multiple apertures was used. However, it forms only two different *effective* field regions (similar to the approach used in Ref. 8); the remaining intermediate apertures merely provide shielding from fringe fields created by the limited-diameter electrodes. Another important purpose of this multi-aperture construction is discussed below.

E. Focusing criteria and performance

Selection of optimal parameters for the ion-optical system described above requires numerical optimization of its

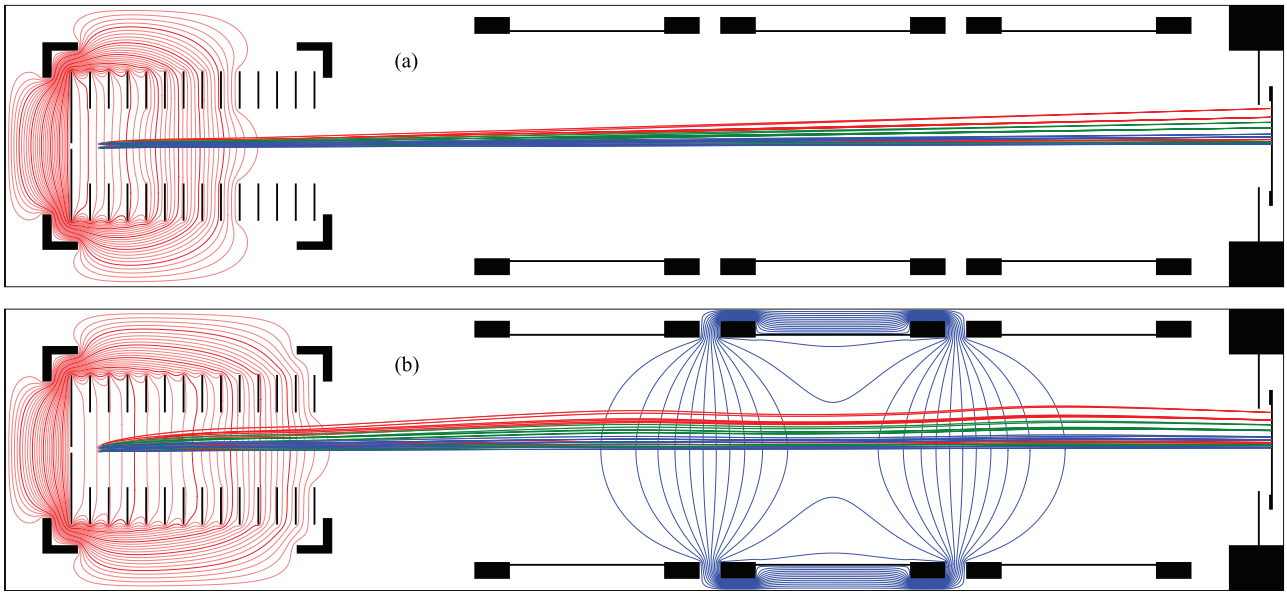

FIG. 2. Cross-section of the ion optics arrangement with illustration of electrostatic potentials and ion trajectories for the extreme operating conditions: (a) lower KE limit ($K_{max} = 0.163$ eV; $L_0 = 40$ mm, $L_1 = 50$ mm, $V_0 = 320$ V, $V_1 = 231.1$ V, $V_L = 0$); (b) upper KE limit ($K_{max} = 6.75$ eV; $L_0 = 75$ mm, $L_1 = 55$ mm, $V_0 = 3000$ V, $V_1 = 1891$ V, $V_L = -6600$ V). In both cases $\Delta\tau_{max} \approx 50$ ns. Trajectories correspond to ions with initial KEs equal to K_{max} (red), $0.4K_{max}$ (green) and $0.1K_{max}$ (blue); see text for details. Equipotential contours are drawn in red for positive potentials (with 10 V steps in (a) and 100 V in (b)) and blue for negative (with 500 V steps).

performance characteristics, such as radial magnification and TOF and radial focusing quality. The definitions of the total TOF stretching and radial magnification are straightforward, but the relevant definition of the resolution of the system requires attention.

First, the ionization region has finite spatial dimensions, and it would be natural to use the experimental distribution to set initial ion positions in the numerical simulations. This distribution is determined by the density distribution in the molecular beam, intensity distributions in the laser beams, and the geometry of their intersection. The expected diameter of the skimmed molecular beam can be used for rough estimation of the extent of the ionization region along the laser beams. The dimensions perpendicular to the laser beams, however, must include not only the actual diameters of the focused laser beams (which are relatively small) but also uncertainties in alignment of these beams relative to the ion optics, if reliable simulations and robust experimental operation are desired. Therefore, the extent of the ionization region used in the simulations reported below was set to 1 mm along the TOF axis (alignment uncertainty) and 2 mm perpendicular to it (molecular beam diameter).

Second, the focusing quality must be equally good over the whole recorded image, that is, for all KEs in the measured KE range. In practice, however, aberrations lead to different blurrings at different radii, and the most relevant characteristic for optimization is the *worst case* blurring. This approach guarantees that for *any* KE in the measured distribution the resolution will be at least as good as the calculated value. Therefore, ions with various initial KEs must be included in the simulations. In the present work a sample of 3 values: K_{max} (KE imaged to the edge of the detector), $0.4K_{max}$ and $0.1K_{max}$, was found to be sufficiently representative.[32] Five angles (starting from 10° with 40° steps) relative to the TOF axis were used for initial directions of the ions.

It should be also noted that in most experiments the primary quantity of interest is the KE distribution (KED) rather than the speed distribution. Therefore, if the radial blurring is denoted by ΔR, minimization of the quantity $R \cdot \Delta R$, which translates to ΔK in the KE scale, is more relevant than minimization of ΔR itself. The relative KE resolution values reported below were determined using this approach as worst-case ΔK divided by K_{max}.

III. RESULTS AND ANALYSIS

A. Optimization of the numerical model

The goal of the optimization for SVMI operation is to find the ion optics parameters that provide the best KE resolution and TOF focusing for a given KE range, such that the image fits into the detector and the TOF stretching is sufficient for slicing. The fact that the radial magnification and TOF dispersion have simple scaling rules with respect to ion mass and applied voltages allows to introduce one variable

$$M \equiv \Delta\tau_{max}\sqrt{K_{max}/m}, \tag{7}$$

referred henceforth as the "magnification index."[33] Its value is completely and unambiguously determined by the experimental conditions: the particle mass m, the desired imaged KE range K_{max} and the TOF stretching $\Delta\tau_{max}$ needed for slicing. Since focusing does not depend on ion mass, representations of the simulation results as a function of the magnification index provide the most convenient way to select the best ion optics parameters for SVMI operation in each particular experiment with ions of any kind.

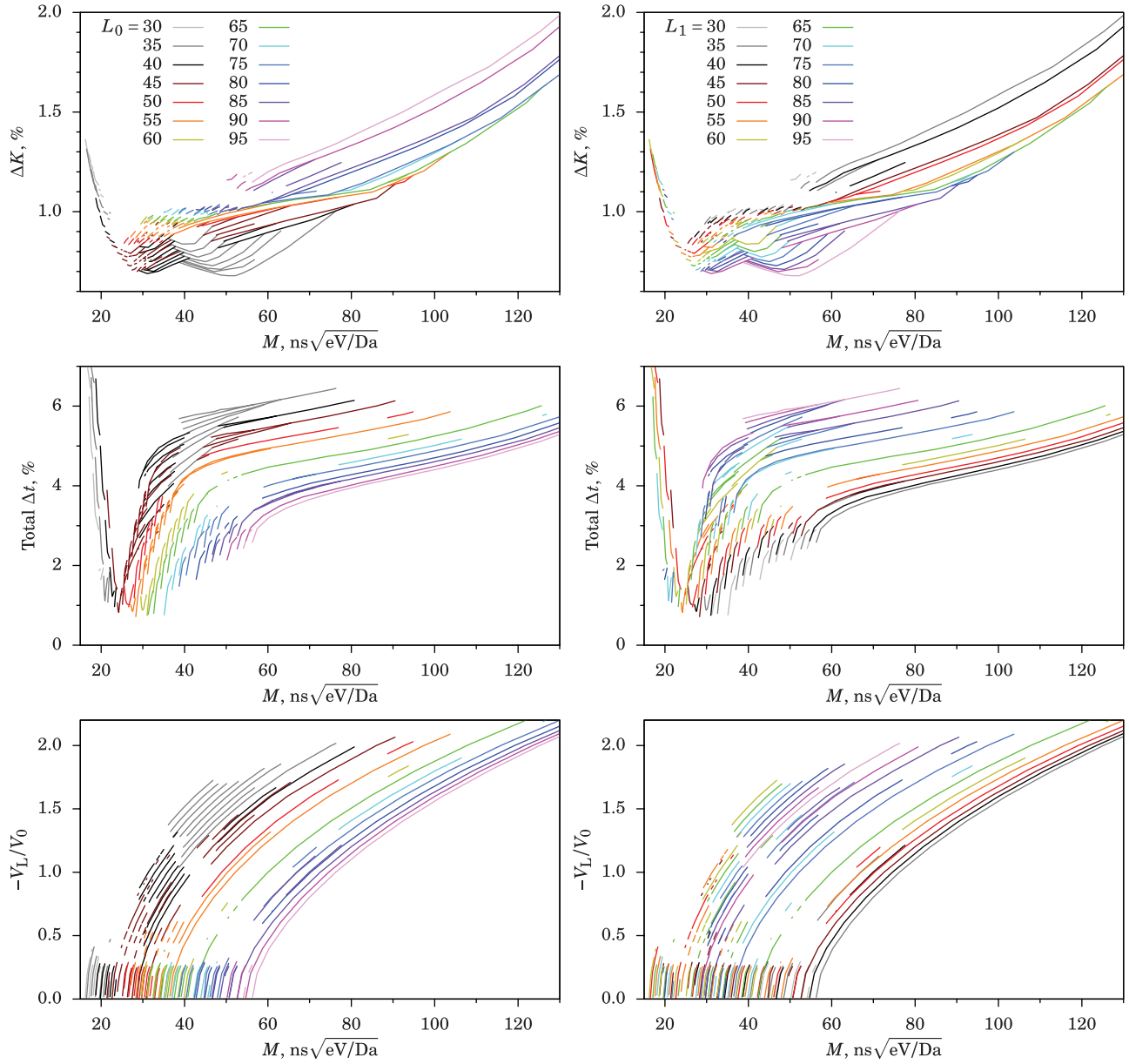

FIG. 3. Pareto-optimal results of numerical simulations plotted as functions of the magnification index M and the effective accelerator lengths L_0 and L_1 (in mm): relative overall kinetic energy (ΔK) and total TOF (Δt) resolutions, and the ratio of the voltages applied to the additional lens (V_L) and the back of the accelerator (V_0). (Both columns show the same set of data, but colored according to L_0 (left) or L_1 (right) values.)

A major difficulty, however, is that *two independent* quantities, namely, the radial and temporal blurrings, need to be minimized. Their *simultaneous* minimization is impossible, since they depend on a common set of ion optics parameters, and hence a trade-off is required. Nevertheless, the variety of parameter values from which the trade-off selection has to be made can be reduced to the so-called Pareto-optimal set,[34] which contains only those combinations of parameter values that cannot be changed without deterioration of at least one characteristic. Thus, selection within the Pareto set allows optimization of performance by favoring certain characteristics at the expense of others. Since in specific experiments different parameters might have different relative importance, the representations of the simulation results chosen here include all (and only) Pareto-optimal results, allowing selection of conditions relevant to each particular case. If more information is available regarding the data being measured and the desired priorities of performance characteristics, additional optimizations can be performed by starting from some relevant point selected from these results.

Figure 3 shows some of the characteristics obtained in the numerical simulations (see Refs. 15 and 16 for a complete set of plots and a detailed description of how they were generated). The most important advantage of the compound lens, as evident from these plots, is that the radial magnification can now be varied over a broad range while keeping reasonably good focusing properties. Namely, for the desired TOF stretching $\Delta\tau_{max} = 50$ ns, the measured KE range of H^+ ions ($m = 1$ Da) can extend from ~0.16 eV to ~6.8 eV (M values ranging from 20 to 130 ns$\sqrt{\text{eV/Da}}$), maintaining KE resolution better than ~2% in this whole range, and even $\lesssim$1% for ranges up to ~2.5 eV.

The difficulty with simultaneous optimization, however, is illustrated by the observation that the parameters that provide the best KE resolution do not correspond to the best TOF resolution. The plotted "total Δt" curve in fact includes the temporal distortion of the central slice,[35] since the total TOF deviations are important for time-sliced detection. In the case of 3D VMI, where the arrival time is measured directly, and the distortions can be easily corrected by data processing, only the TOF blurring ("Δt") determines the temporal resolution. Its magnitude is a few times smaller ($\lesssim 1\%\ldots 2\ \%$, see plots in Refs. 15 and 16), but of course it still exhibits the same behavior relative to the radial resolution (ΔK). As mentioned above, the "best" trade-off decision in selecting among these Pareto-optimal combinations of parameter values depends on the details of each particular experiment and must be made by the investigator. For example, in experiments with focused (and precisely positioned) laser beams the ionization region extent along the TOF axis is much smaller than the 1 mm used in the simulations, and hence the TOF blurring should be negligible compared to the plotted worst case. That is, the optimal parameters can be chosen based solely on the best KE resolution, ignoring the "Δt" plot.

In spite of these optimization challenges, the positive role of the additional lens in the magnification variation can be seen clearly from the plots of the voltage applied to the lens compared to the accelerator voltage (V_L/V_0). It is evident that for low M values (larger radial magnifications at a given TOF stretching) the Pareto-optimal solutions include operation without the additional lens ($V_L \to 0$), but above a certain M value (that is, for reduced radial magnifications, or equivalently, extended TOF stretchings at a given radial magnification) all Pareto-optimal variants require the use of the lens. As the optical power of the lens grows with the applied voltage, the resulting radial magnification of the system decreases, allowing SVMI measurements for larger KEs. However, at the same time the aberrations increase with the lens power, so the resolution deteriorates monotonically.

Another important observation from the plots is that different operating regimes require different combinations of the accelerator lengths L_0 and L_1. As mentioned above, mechanical motion of the apertures to satisfy these requirements would be impractical. Nevertheless, construction of the accelerator with multiple intermediate apertures, as shown in Fig. 2, offers a simple solution to this problem by allowing purely electrical commutations of the applied voltages. Numerical simulations demonstrate that the effective length of the electric field regions can be changed not only in multiples of the inter-electrode distances (10 mm in the present case) but even *continuously* by appropriate interpolation of the intermediate voltages. In practice this requires high-voltage potentiometers, but for simplicity our current implementation uses a voltage divider assembled from fixed resistors that allows L_0 and L_1 variations in 5 mm steps, which provides sufficiently fine control.

It should be noted that the optimizations described above were not quite complete. For example, the accelerator aperture diameters, as well as the position and the thickness of the additional lens, were not fully optimized. However, several test simulations with relatively small variations of these parameters did not exhibit significant improvements of performance characteristics, indicating that a complete numerical optimization of all parameters within the selected optical scheme, being a much more computationally expensive effort, is unlikely to yield noticeable benefits.

B. Experimental examples

The SVMI system built according to the design discussed above has been successfully used for detection of H fragments with KEs $\lesssim 0.4$ eV in the experiments on overtone-induced dissociation and isomerization of the hydroxymethyl radical (CH_2OH and CD_2OH).[36] The details and most important results of those studies are given in that publication (two examples for H and D detection are also included in the supplementary material[29]). Here, for demonstration of the system capabilities, we provide some results of auxiliary measurements performed for the much more energetic (KE $\lesssim 2$ eV) byproducts. However, because this case involved polyatomic cofragments with relatively large densities of states, the H fragment KE distributions were broad and thus not very suitable for demonstration of the instrumental resolution. Therefore, a few examples of other experiments with smaller molecules used for tests and characterization of the newly built system are also presented here.

Figure 4(a) shows a sliced velocity map image of O^+ fragments produced by multiphoton photodissociation and ionization of O_2 in a one-laser experiment at $\nu \approx 44\,444\ \mathrm{cm}^{-1}$ ($\lambda_{vac} \approx 225$ nm), which is often used for characterization of VMI setups.[3,8] Due to the relatively large mass of the O^+ ion, the TOF spread even without using the additional lens was ~80 ns, already sufficient for slicing. The same image taken with the lens, with ~130 ns stretching, had very similar appearance but lower intensity because a smaller fraction of the ion cloud (thinner slice) was recorded.

As can be seen from comparison of the KEDs extracted from these images (Fig. 4(b)) the use of the lens did not affect the experimental resolution.[37] A small discrepancy between the positions of the peaks, however, is noticeable in the high-KE part of the distributions. The origin of this difference is that the calibration of the mapping between the initial radial velocities and the radii in the image was done using *only* the numerical simulations of the ion-optical system. Nevertheless, the differences between the obtained calibration and the peak positions predicted from the known energetics of the processes did not exceed ~1%–2% neither in these nor in other test cases, some of which are illustrated below. Taking into account that all ion optics parameter values were also set according to the simulation results (experimental variations around these values showed that they indeed provide the best radial and temporal focusing, which was tested by displacing the focused laser beam perpendicular to and along the TOF axis[29]), this offers the valuable advantage of selecting the most suitable operating conditions for each particular experiment without the need for tedious experimental calibrations and optimizations of the SVMI system.

Results of two SVMI test experiments with H fragments are presented in Fig. 5. The neutral H fragments were ionized by $1 + 1'$ resonance-enhanced multiphoton

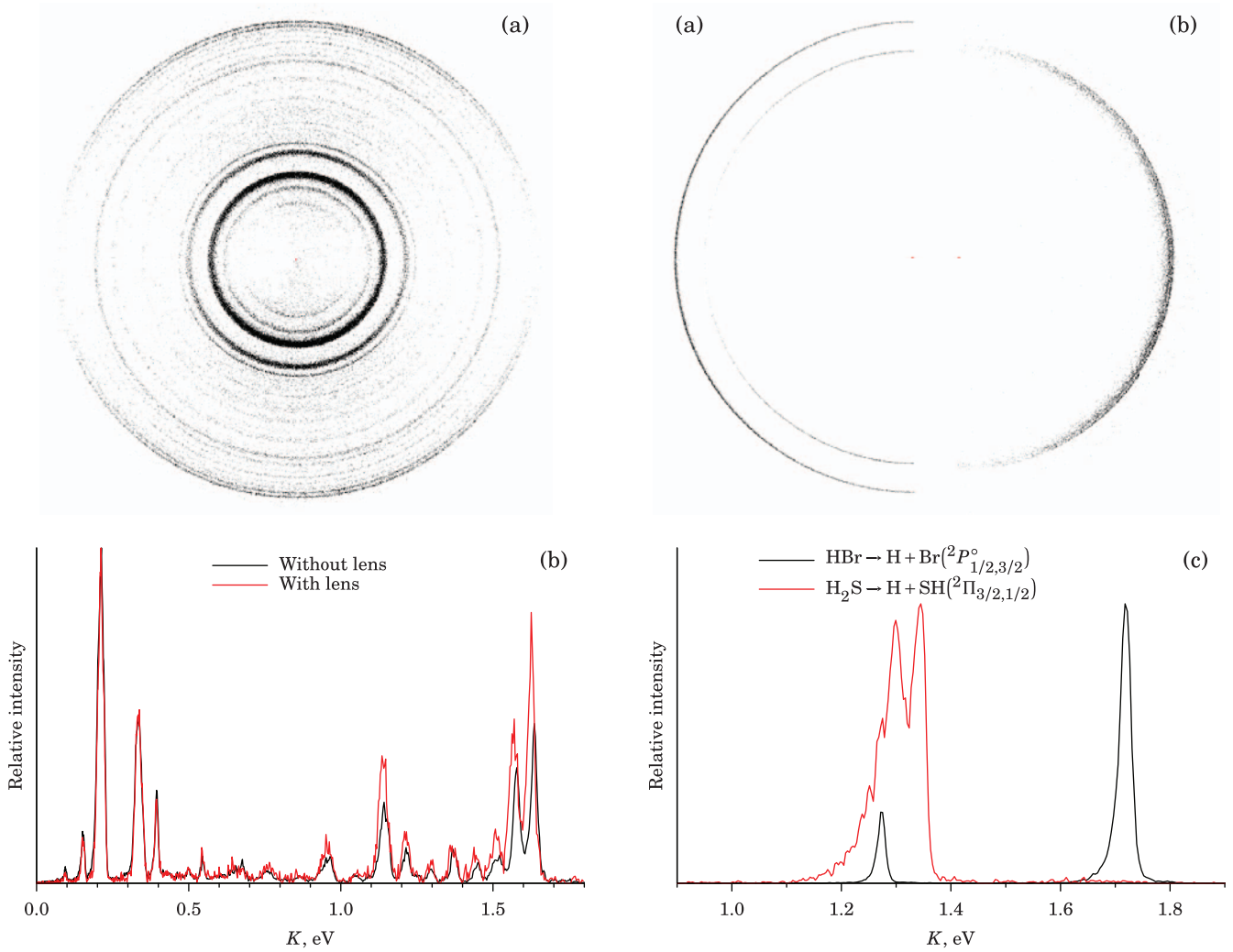

FIG. 4. Distribution of O^+ ions in the photoinitiated reaction $O_2 \xrightarrow{4h\nu} O + O^+ + e^-$ at $\nu \approx 44\,444$ cm^{-1}. (a) Raw sliced velocity map image (with vertical laser polarization) recorded without the additional lens. (b) Comparison of KEDs extracted from SVMI data recorded with and without the lens.

FIG. 5. Distributions of H fragments in photodissociation of HBr and H_2S. (a) and (b) show raw SVMI data for $HBr \xrightarrow{h\nu} H + Br(^2P^\circ_{1/2,3/2})$ and $H_2S \xrightarrow{h\nu} H + SH(^2\Pi_{3/2,1/2}, v = 0, J)$ processes, specifically (only one half of each symmetric image is shown). (c) KEDs extracted from these data.

ionization using Ly-α radiation produced by frequency tripling of 364.8 nm radiation in an Ar/Kr gas cell for excitation of the $2p$ state and the unconverted radiation for further near-threshold ionization.[17] This ionization scheme leads to negligible electron recoil and hence avoids additional blurring. Due to a relatively narrow ionization laser bandwidth, it was scanned over the full Doppler profile of the H fragments. One of the experiments is HBr photodissociation at $\nu \approx 44\,444$ cm^{-1}, which produces two monochromatic peaks corresponding to the Br cofragment in either the ground electronic state ($^2P^\circ_{3/2}$) or the spin–orbit excited state ($^2P^\circ_{1/2}$). The other is H_2S photodissociation at $\nu \approx 42\,560$ cm^{-1}, producing close-lying and rotationally broadened peaks corresponding to the SH cofragment in the spin–orbit sublevels of its ground electronic state ($X\,^2\Pi_{1/2,\,3/2}$). In these cases the TOF stretching without the additional lens was only ~20 ns, clearly insufficient for good slicing with a ~5 ns pulse. With the additional lens, however, it became possible to increase the TOF stretching to 50 ns without overfilling the detector. The peaks in the HBr experiment (Fig. 5(c)) show halfwidths of ~20 meV, demonstrating a relative KE resolution of ~1.2%, in good agreement with the numerical simulations.[38] The two peaks in the H_2S experiment, which are ~47 meV (~2.5%) apart, demonstrate that such features are also well-resolved despite the partial overlap of their rotational envelopes.

Finally, Fig. 6 shows a comparison of full-projection VMI (a) and SVMI (b) measurements of H fragment KEDs in one-photon dissociation of the CH_2OH radical at $\nu \approx 27\,420$ cm^{-1} ($\lambda_{vac} = 3$Ly-$\alpha \approx 364.7$ nm). The high-KE part consists of several peaks corresponding to vibrational excitations in the CH_2O cofragment, broadened by relatively high rotational excitation. The low-KE part contains a continuous background of yet unidentified origin. As can be seen, these distributions also look very similar in terms of the KE resolution. However, the distribution reconstructed from the full-projection image (using BASEX[39]) is much noisier, especially towards the low-KE end, whereas the distribution extracted from the sliced image (by weighted angular integration) exhibits good signal-to-noise ratio everywhere.

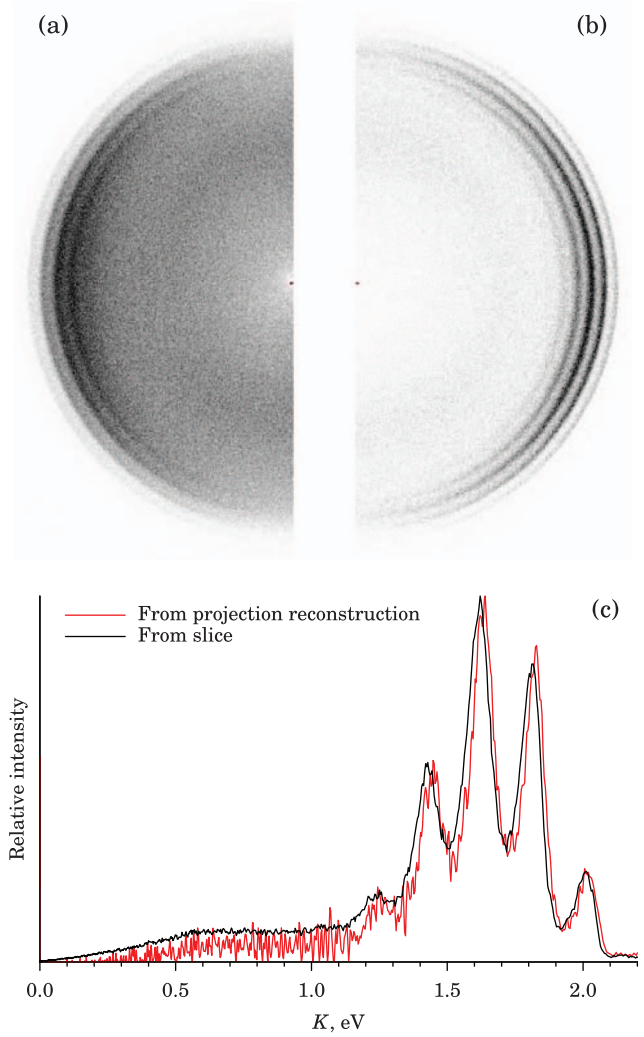

FIG. 6. H fragment distribution in CH_2OH dissociation after electronic excitation at $\nu \approx 27\,420\ cm^{-1}$ ($\lambda_{vac} = 3Ly\text{-}\alpha$). (a) Raw full-projection VMI data. (b) Raw SVMI data. (c) Comparison of KEDs extracted from these data. Notice the significantly worse signal-to-noise ratio in the full-projection reconstruction despite longer data accumulation.

The difference in intensities of the signal at KEs $\lesssim 1$ eV is likely caused by non-uniformity in the detection efficiency. Namely, reconstruction by application of inverse Abel transform to the full-projection image subtracts high-KE contributions from the low-KE signal, and therefore if the central part of the detector has decreased sensitivity,[40] the reconstructed KED becomes negatively biased in the lower KE range (as evident for $K \lesssim 0.3$ eV in Fig. 6(c)). From this perspective, the KED extracted from the SVMI data is also more reliable intensity-wise than the KED reconstructed from the full-projection VMI data.

Further experimental studies of CH_2OH dissociation after electronic excitation at higher photon energies are currently performed in our laboratory. The maximum KE of H fragments corresponding to the lowest dissociation channel ($H + CH_2O$) in these experiments reaches >3 eV, while other channels (corresponding to HCOH and triplet CH_2O cofragments) opening with increase in the excitation energy lead to H fragments with rather low KEs. Nevertheless, the SVMI system exhibits good performance (consistent with the simulations) even in these complicated situations.

IV. DISCUSSION AND CONCLUSION

The results of the numerical simulations and experimental tests presented above demonstrate the success of our ion-optical scheme in application to SVMI of H photofragments. Its flexibility allows operation in a broad range of kinetic energies (more than one order of magnitude), exhibiting high resolution comparable to that of other modern VMI and SVMI systems (even those incapable of H^+ SVMI).

Due to the difficulties in SVMI of the light H fragments discussed above, very few examples of such experiments can be found in the literature. In one example using the electrostatic approach,[11] slicing of H fragments distribution was demonstrated with a test case of HBr photodissociation. The employed system, however, used a ø120 mm detector (significantly more expensive than the ø40 mm detector used in the present work), and nevertheless the slice was relatively thick, containing 30–40 ns out of the 150 ns TOF spread of the ion cloud. SVMI of H fragments was also demonstrated using the delayed extraction approach. The first experiments[10] with HBr photodissociation achieved relatively modest velocity resolution of 1.5%, that is ~3% in the KE scale. In more recent work employing a simpler ion optics design[12] this was improved to some extent, although the KEDs broadened by electron recoil did not allow reliable determination of the achieved instrumental resolution. The quoted velocity resolution "on the order of 1% or better" corresponds to ~2% in the KE scale, still worse than most results of the present work. Moreover, each of the cited works used quite limited KE ranges and did not discuss the applicability limits of their setups. Examples of other slicing methods, such as the Doppler slicing approach,[41] did not demonstrate better effective resolution either and have more limited applicability than the time-sliced VMI.

It should be noted that the use of an additional lens in the drift region for improved radial magnification control is not new for VMI setups. In most cases this arrangement was used to *increase* the magnification in experiments with low-KE fragments,[42–44] but there are examples[13,45] where the goal was to fit images of high-KE distributions into a limited-size detector. However, all of these works employed only full-projection VMI operation and thus were not concerned with the temporal properties of their systems, which are crucial for the SVMI operation considered in the present work. The ion optics aberrations and their effect on the final resolution also have not been addressed sufficiently in these previous works (except Ref. 13, where nevertheless the geometry optimization was done solely by numerical means, without providing general insights).

Our conclusion that the numerical model of the present system provides a very reliable description of system performance greatly facilitates selection of optimal ion optics parameters in each experiment. Moreover, it suggests that more complicated ion-optical arrangements can be developed and operate robustly within this approach. Namely, the present system is rather minimalistic, including only the parts that are

indispensable for TOF and radial focusing and radial magnification control. Addition of more ion-optical elements (more than two field regions in the accelerator, compound lens in the drift region) is likely to improve the achievable resolution and extend the operating limits of the system. Although this will increase the number of parameters that must be set experimentally during system operation, the values of all these parameters can be reliably obtained from the simulations, so that no additional experimental tuning or calibration would be necessary.

One such promising modification is the use of electrically biased detector entrance. In the present system the front plate of the detector, as well as the exit of the accelerator, is grounded in order to avoid electric fields between them and the vacuum chamber walls. As a result, the kinetic energies of ions arriving at the detector are limited by the voltage applied to the accelerator, which might be relatively low, leading to decreased detection efficiency. Creating an electric potential difference between these parts might be used for increasing the kinetic energies of the ions before they hit the detector. Moreover, appropriate shaping of the created electric field might be employed for additional magnification control.

It should be noted that while the ion optics system presented here was developed specifically for SVMI of H fragments, its advanced temporal characteristics might be usable in other applications as well. For example, it should permit or enhance the performance of 3D VMI in cases where absolute time resolution is limited by the nature of the experiment (for example, by the use of nanosecond lasers, as in our case) or the detector response time. The controllable TOF stretching can then be used to improve the relative time resolution and hence the axial velocity resolution of the system. This might be especially important in 3D VMI of photoelectrons, which have substantial kinetic energies and at the same time require picosecond detection resolution.

ACKNOWLEDGMENTS

The authors are grateful to Dr. András Kuthi from the Pulsed Power Laboratory at USC for the suggestion of the fast high-voltage pulser design and his help in its adaptation to our needs. This article is based upon work supported by the National Science Foundation under Grant No. CHE-0951976, and the Division of Chemical Sciences, Geosciences, and Biosciences of the Department of Energy, Basic Energy Sciences, under Grant No. DE-FG02-05ER15629.

[1]M. N. R. Ashfold, N. H. Nahler, A. J. Orr-Ewing, O. P. J. Vieuxmaire, R. L. Toomes, Th. N. Kitsopoulos, I. A. Garcia, D. A. Chestakov, S.-M. Wu, and D. H. Parker, Phys. Chem. Chem. Phys. **8**, 26 (2006).
[2]A. I. Chichinin, K.-H. Gericke, S. Kauczok, and C. Maul, Int. Rev. Phys. Chem. **28**, 607 (2009).
[3]A. T. J. B. Eppink and D. H. Parker, Rev. Sci. Instrum. **68**, 3477 (1997).
[4]D. W. Chandler and P. L. Houston, J. Chem. Phys. **87**, 1445 (1987).
[5]*Imaging in Chemical Dynamics*, ACS Symposium Series Vol. 770, edited by A. G. Suits and R. E. Continetti (American Chemical Society, 2000).
[6]*Imaging in Molecular Dynamics: Technology and Applications*, edited by B. J. Whitaker (Cambridge University Press, 2003).
[7]Ch. R. Gebhardt, T. P. Rakitzis, P. C. Samartzis, V. Ladopoulos, and Th. N. Kitsopoulos, Rev. Sci. Instrum. **72**, 3848 (2001).
[8]J. J. Lin, J. Zhou, W. Shiu, and K. Liu, Rev. Sci. Instrum. **74**, 2495 (2003).
[9]D. Townsend, M. P. Minitti, and A. G. Suits, Rev. Sci. Instrum. **74**, 2530 (2003).
[10]R. L. Toomes, P. C. Samartzis, T. P. Rakitzis, and T. N. Kitsopoulos, Chem. Phys. **301**, 209 (2004).
[11]W. Li, S. D. Chambreau, S. A. Lahankar, and A. G. Suits, Rev. Sci. Instrum. **76**, 063106 (2005).
[12]V. Papadakis and Th. N. Kitsopoulos, Rev. Sci. Instrum. **77**, 083101 (2006).
[13]G. A. Garcia, L. Nahon, Ch. J. Harding, E. A. Mikajlo, and I. Powis, Rev. Sci. Instrum. **76**, 053302 (2005).
[14]Previous VMI designs employing additional lenses after the primary acceleration region (see Refs. 7, 9, 13, and 42 for the most important examples) used them for a different purpose and/or in a different configuration resulting in inferior performance.
[15]M. Ryazanov, "Development and implementation of methods for sliced velocity map imaging. Studies of overtone-induced dissociation and isomerization dynamics of hydroxymethyl radical (CH_2OH and CD_2OH)," Ph.D. dissertation, University of Southern California, 2012.
[16]M. Ryazanov, "Design and implementation of an apparatus for sliced velocity map imaging of H atoms," 2012, see http://www-bcf.usc.edu/~reisler/assets/pdf/SVMI.pdf.
[17]D. G. Conroy, "Rydberg state of an open shell species: Characterization and photophysics of the $3p_z$ state of CH_2OH," Ph.D. dissertation, University of Southern California, 2000.
[18]V. Dribinski, "Photoelectron and ion imaging studies of the mixed valence/Rydberg excited states of the chloromethyl radical, CH_2Cl, and the nitric oxide dimer, $(NO)_2$," Ph.D. dissertation, University of Southern California, 2004.
[19]D. A. Chestakov, S.-M. Wu, G. Wu, D. H. Parker, A. T. J. B. Eppink, and Th. N. Kitsopoulos, J. Phys. Chem. A **108**, 8100 (2004).
[20]W. C. Wiley and I. H. McLaren, Rev. Sci. Instrum. **26**, 1150 (1955).
[21]D. A. Dahl, Int. J. Mass Spectrom. **200**, 3 (2000).
[22]SIMION 8.0, 2010, see http://www.simion.com.
[23]Yu. A. Kotov, G. B. Mesyats, S. N. Rukin, A. L. Filatov, and S. K. Lyubutin, in *Digest of Technical Papers: Ninth IEEE International Pulsed Power Conference* (IEEE, Albuquerque, NM, 1993), Vol. 1, pp. 134–139.
[24]A. Kuthi, P. Gabrielsson, M. R. Behrend, P. Th. Vernier, and M. A. Gundersen, IEEE Trans. Plasma Sci. **33**, 1192 (2005).
[25]M. L. Lipciuc, A. J. van den Brom, L. Dinu, and M. H. M. Janssen, Rev. Sci. Instrum. **76**, 123103 (2005).
[26]M. L. Lipciuc and M. H. M. Janssen, Phys. Chem. Chem. Phys. **8**, 3007 (2006).
[27]If the slicing pulse has fixed duration, as in the present work. In general, fast pulsers with adjustable pulse width are either slower or more complicated.
[28]M. L. Lipciuc, J. B. Buijs, and M. H. M. Janssen, Phys. Chem. Chem. Phys. **8**, 219 (2006).
[29]See supplementary material at http://dx.doi.org/10.1063/1.4798929 for relative magnification equations, focusing tests, and additional experimental examples.
[30]In principle, the radial magnification can be changed by moving the detector closer to or farther from the accelerator. While this approach was implemented in some systems (for example, Ref. 45), it is cumbersome from a mechanical point of view, requiring long-stroke movements of high-voltage parts in a high-vacuum system. The desire to find *one best* position of the lens here stems from the same mechanical argument.
[31]This number resulted simply from the dimensions of the existing vacuum chamber and the length of the standard nipple used for its extension. It does not carry any particular importance.
[32]The proportionality factors 1, 0.4, and 0.1 were chosen for relatively uniform covering of the *speed* space and hence the radial direction in the image.
[33]This quantity is not directly related to the relative magnification M_{rel} discussed above. Rather, the index describes the combination of the temporal and radial characteristics and is numerically equal to the total TOF stretching for a distribution of H^+ ions ($m = 1$ Da) with $K_{max} = 1$ eV under voltages scaled such that the image fills the whole detector.
[34]K. Deb, in *Search Methodologies*, edited by E. K. Burke and G. Kendall (Springer, US, 2005), pp. 273–316.
[35]As can be seen from Fig. 2, ions that are mapped to the outer part of the image travel somewhat longer paths than ions with $K_0 \approx 0$, and their average velocity inside the lens is somewhat lower due to the electric field configuration. This means that ions with zero axial velocity (the central slice of the distribution), which in perfect VMI must reach the detector simultaneously, arrive at somewhat different times depending on their radial velocity components.

[36]M. Ryazanov, Ch. Rodrigo, and H. Reisler, J. Chem. Phys. **136**, 084305 (2012).
[37]The lower signal-to-noise ratio in the data "with lens" is due to the mentioned lower signal intensity. The differences in relative intensities of several peaks in the distributions were not reproducible, being apparently caused by small laser power variations between these experiments and different power dependences of different O^+-producing channels in this highly nonlinear 4-photon process.
[38]The slightly asymmetric shape of the peaks, with a longer wing on the lower-KE side, is due to the finite slice thickness. See Refs. 15 or 16 for more details.
[39]V. Dribinski, A. Ossadtchi, V. A. Mandelshtam, and H. Reisler, Rev. Sci. Instrum. **73**, 2634 (2002).
[40]The detector used in the present work has been used before in experiments which produced large intensities near the image center, leading to some deterioration of the MCP gain in that area.
[41]C. Huang, S. A. Lahankar, M. Hwa Kim, B. Zhang, and A. G. Suits, Phys. Chem. Chem. Phys. **8**, 4652 (2006).
[42]H. L. Offerhaus, C. Nicole, F. Lépine, C. Bordas, F. Rosca-Pruna, and M. J. J. Vrakking, Rev. Sci. Instrum. **72**, 3245 (2001).
[43]M. M. Harb, S. Cohen, E. Papalazarou, F. Lépine, and C. Bordas, Rev. Sci. Instrum. **81**, 125111 (2010).
[44]Y. Zhang, C.-H. Yang, S.-M. Wu, A. van Roij, W. J. van der Zande, D. H. Parker, and X. Yang, Rev. Sci. Instrum. **82**, 013301 (2011).
[45]E. Wrede, S. Laubach, S. Schulenburg, A. Brown, E. R. Wouters, A. J. Orr-Ewing, and M. N. R. Ashfold, J. Chem. Phys. **114**, 2629 (2001).